

SANDIA REPORT

SAND91-0285 • UC-528

Unlimited Release

Printed July 1992

AD-A254 944



1

The Delayed Gamma Environment Produced by Exoatmospheric Nuclear Weapons Detonation...

Barry L. Spletzer

S DTIC
ELECTE
SEP 01 1992
A D

Prepared by
Sandia National Laboratories
Albuquerque, New Mexico 87185 and Livermore, California 94550
for the United States Department of Energy
under Contract DE-AC04-76DP00789

This document has been approved
for public release and sale; its
distribution is unlimited.

Issued by Sandia National Laboratories, operated for the United States Department of Energy by Sandia Corporation.

NOTICE: This report was prepared as an account of work sponsored by an agency of the United States Government. Neither the United States Government nor any agency thereof, nor any of their employees, nor any of their contractors, subcontractors, or their employees, makes any warranty, express or implied, or assumes any legal liability or responsibility for the accuracy, completeness, or usefulness of any information, apparatus, product, or process disclosed, or represents that its use would not infringe privately owned rights. Reference herein to any specific commercial product, process, or service by trade name, trademark, manufacturer, or otherwise, does not necessarily constitute or imply its endorsement, recommendation, or favoring by the United States Government, any agency thereof or any of their contractors or subcontractors. The views and opinions expressed herein do not necessarily state or reflect those of the United States Government, any agency thereof or any of their contractors.

Printed in the United States of America. This report has been reproduced directly from the best available copy.

Available to DOE and DOE contractors from
Office of Scientific and Technical Information
PO Box 62
Oak Ridge, TN 37831

Prices available from (615) 576-8401, FTS 626-8401

Available to the public from
National Technical Information Service
US Department of Commerce
5285 Port Royal Rd
Springfield, VA 22161

NTIS price codes
Printed copy: A03
Microfiche copy: A01

SAND91-0285
Unlimited Release
Printed July 1992

Distribution
Category UC-528

THE DELAYED GAMMA ENVIRONMENT PRODUCED
BY
EXOATMOSPHERIC NUCLEAR WEAPONS DETONATION

Barry L. Spletzer
Containment Technology
Sandia National Laboratories
Albuquerque, New Mexico 87185

Accession For	
NTIS CRA&I	<input checked="" type="checkbox"/>
DTIC TAB	<input type="checkbox"/>
Unannounced	<input type="checkbox"/>
Justification	
By _____	
Distribution/ _____	
Availability Codes	
Dist	Avail and/or Special
A-1	

Abstract

DTIC QUALITY INSPECTED 3

The production of delayed gamma ray radiation from the debris following a nuclear weapon detonation in space can produce an environment that is detrimental to various sensor systems on space-based assets. This report examines the nature of this delayed gamma environment and provides guidelines for assessing its severity.

A full derivation of the environment is presented based on a simple symmetric model. Included in the environment are single burst and multiburst scenarios and an estimate of the radiation resulting from the distributed weapon debris and the debris plated out on the space-based asset. All results are presented in parametric form to allow them to be applied directly to a wide range of engagement scenarios.

A brief discussion of the nature of required shielding to survive a gamma environment is presented. Methods of mitigating the radiation environment are discussed. The report concludes that levels in excess of 10^{11} MeV/(cm²·s) per cal/cm² x-ray will exist for several seconds after a burst. In the event of a multiburst scenario, gamma dose rates of approximately 10^{12} MeV/(cm²·s) can be expected for each cal/cm² per second of prompt dose received during the time of the scenario. These results show that it will be necessary to provide mitigation of the debris environment or shielding against it to achieve functional sensor systems during a nuclear engagement.

92 8 31 023

315300

92-24113



3609

CONTENTS

Section		Page
1.	INTRODUCTION	1
2.	BASIC DEBRIS RADIATION RELATIONSHIPS	1
3.	SINGLE BURST BACKGROUND ENVIRONMENT	2
4.	MULTIBURST BACKGROUND ENVIRONMENT	6
5.	PLATEOUT RADIATION ENVIRONMENT	8
6.	MULTIBURST PLATEOUT ENVIRONMENT	13
7.	COMBINED DEBRIS RADIATION ENVIRONMENT	16
8.	DEBRIS ENVIRONMENT APPLICATION	22
9.	MITIGATION OF DEBRIS RADIATION ENVIRONMENT	22
10.	SUMMARY AND CONCLUSIONS	26
11.	REFERENCE.....	28

LIST OF FIGURES

Figure		Page
1.	Schematic of the Debris Radiation Environment	3
2.	Single Burst Background Debris Environment	7
3.	Multiburst Background Debris Environment	9
4.	Parametric Multiburst Background Debris Environment	10
5.	Single Burst Plateout Debris Environment	12
6.	Parametric Single Burst Plateout Debris Environment	14
7.	Parametric Multiburst Plateout Debris Environment	15
8.	Multiburst Plateout Debris Environment	17
9.	Single Burst Total Debris Environment	18
10.	Comparison of Calculated and Approximated Dose Rates for a Single Burst With $Z = 1$ s	20
11.	Multiburst Total Debris Environment	21
12.	Required Uranium Shielding for a 1-cm Sensor	24
13.	Background Debris Dose for a 1-MT Burst	27

1. INTRODUCTION

Recently, considerable effort has been expended on the development of space-based assets that can survive a nuclear weapon attack. Generally, this effort is focused on the prompt nuclear weapon effects; these being hot x-rays, cold x-rays, neutrons and prompt gamma rays. However, delayed weapon effects must also be considered in the balanced hardening of space-based assets to attack. The two delayed effects of greatest interest are the gamma radiation resulting from decay of the weapon debris and radiation from energetic electrons trapped in the earth's magnetic field. This report deals with the gamma radiation produced by decaying weapon debris and provides a number of parametric relationships that can be used to estimate the debris radiation environment for many nuclear weapons attacks scenarios.

In general, the dose rate caused by debris radiation is several orders of magnitude lower than that caused by the prompt weapon effects. However, this dose continues for several seconds to several minutes after the detonation and can be a source of concern for the space-based asset designer. Specifically, the radiation can become an unacceptable source of noise for focal plane arrays and other detectors. For this reason, the level of debris gamma radiation is of considerable interest. However, since detectors are normally rated by the order of magnitude of the radiation dose rate under which they can operate (i.e., 10^8 MeV/(cm²·s)), a relatively rough estimate of the debris gamma environment will suffice to determine the required level of shielding or the needed gamma tolerance of detectors expected to operate in the environment.

2. BASIC DEBRIS RADIATION RELATIONSHIPS

During the detonation of a nuclear weapon, a typical fission releases approximately 200 MeV. Of this energy, about 3% to 5% eventually is emitted as gamma radiation from the decaying weapon debris. The time dependence of the release rate of this radiation is usually of the form given in Equation (1).

$$A(t) = \frac{G}{(1 + t)^{1.2}}, \quad (1)$$

where the time, t , is expressed in seconds since the burst. Glasstone¹ states that the exponent of 1.2 has been observed to vary from 0.9 to 2.0. G may be evaluated by integrating the above expression over time and setting the result equal to the 3% to 5% of the 200 MeV total fission energy.¹ This yields a value of G , which ranges from 1.2 to 2.0 MeV/(fission·second). The exact value chosen in this range only has a negligible effect on the results. However, for the purposes of this report, a value of G equal to 1.9 MeV/(fission·second) has been chosen. Using the fact that 1 kiloton (kT) of explosive yield is equal to 1.45×10^{23} fissions, the value of G can also be expressed as 2.8×10^{23} MeV/(kT·s).

Since the output of a burst is approximately 80% x-rays¹ and a kiloton is defined as 10^{12} calories, a constant J can be defined in a way that relates the fluence received (F) to the yield (Y) and distance from a burst (R):

$$F = \frac{JY}{R^2},$$

$$J = \frac{FR^2}{Y} = \frac{0.8 \times 10^{12} \text{ cal}}{4\pi R^2 kT} R^2,$$

$$J = 6.4 \times 10^{10} \frac{\text{cal}}{\text{kT}}. \quad (2)$$

The remainder of the weapon energy (20%) appears as kinetic energy of the debris.¹ This can be converted directly to debris velocity by

$$E_K = \frac{1}{2} m v^2,$$

$$0.20 B = \frac{E_K}{m} = \frac{1}{2} v^2, \quad (3)$$

where B is the energy/mass ratio of the weapon. A ratio of 1 kT/kg corresponds to a velocity of 1.3×10^6 m/s while a ratio of 0.01 kT/kg results in 1.3×10^5 m/s. So, for a wide range of weapon and weapon delivery geometries, a range of debris velocity from 10^5 to 10^6 m/s can be assumed.

The debris environment can be considered to consist of a thin, expanding spherical shell with the activity and velocity stated above. The spherical shell assumption is not entirely correct, since magnetic fields affect the propagation and shape of the shell. However, it will be used here to provide a rough estimate of the environment because of its relative simplicity and because debris gamma affects are only sensitive to order of magnitude changes in the environment. The activity of the shell can be determined by dividing the total gamma activity by the area for a shell radius S:

$$K(t) = \frac{A(t)Y}{4\pi S^2}, \quad (4)$$

where K(t) represents the areal activity of the shell in units such as MeV/(cm²·s) and Y is the burst yield in kT.

This shell affects the space-based asset in two ways. First, direct radiation from the shell is received. Second, when the shell passes the asset, the radioactive material can plate out on the surface, providing residual radiation long after the shell has passed. The nature of these two environments will be derived separately.

3. SINGLE BURST BACKGROUND ENVIRONMENT

The geometry of the expanding shell with relation to the space-based asset is presented in Figure 1. To determine the dose rate at any time, an integral of the dose provided by a differential shell area must be performed. The differential dose rate is

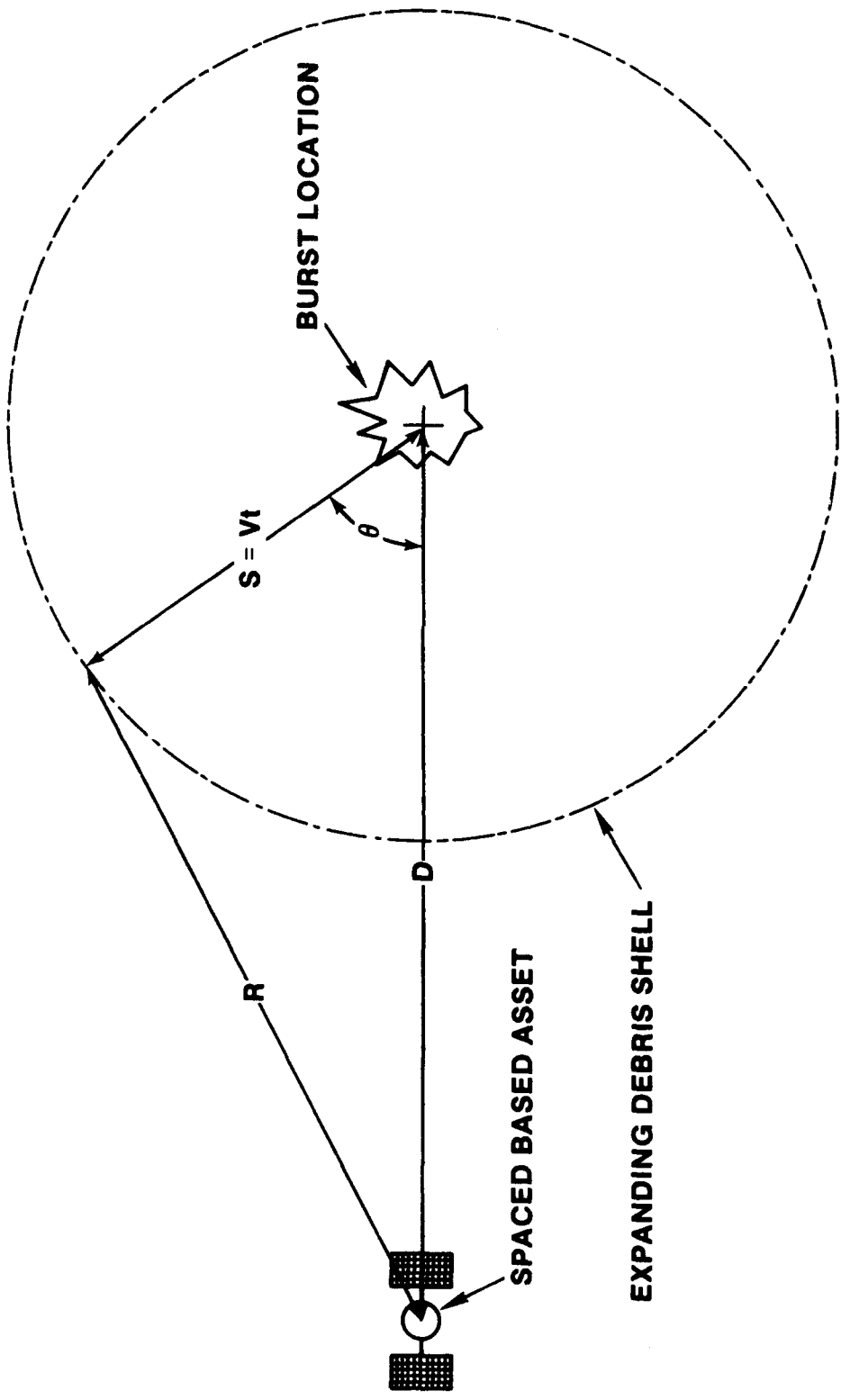


Figure 1. Schematic of the Debris Radiation Environment

$$dI = \frac{K(t)dA}{4\pi R^2}, \quad (5)$$

which is the total activity of a differential area divided by the area over which the radiation is distributed at the distance to the target.

The differential area dA can be chosen as a ring element equidistant from the asset. This is

$$dA = (2\pi S \sin\theta) (Sd\theta) = 2\pi S^2 \sin\theta d\theta. \quad (6)$$

By the law of cosines, R can be expressed in terms of D , S , and θ :

$$R^2 = S^2 + D^2 - 2SD \cos\theta, \quad (7)$$

where D is the distance from the burst to the target, R is the distance from the debris element to the target, S is the radius of the expanding debris shell, and θ is the angle between D and S (see Figure 1). The integral for the dose rate is set up as follows:

$$I = \int \frac{K(t)dA}{4\pi R^2} = \int_0^\pi \frac{K(t)S^2 \sin\theta d\theta}{2(S^2 + D^2 - 2SD \cos\theta)}. \quad (8)$$

Or in terms of R :

$$I = \frac{K(t)S}{2D} \ln \left(\frac{R_{\max}}{R_{\min}} \right). \quad (9)$$

$K(t)$ is replaced with the activity of the source as follows:

$$I = \frac{A(t)Y}{16\pi SD} \ln \frac{(S+D)^2}{(S-D)^2},$$

$$I = \frac{A(t)Y}{8\pi SD} \ln \left(\frac{R_{\max}}{R_{\min}} \right). \quad (10)$$

These two expressions are equivalent. Both expressions exhibit behavior that must be evaluated as a limit for time zero (i.e., $S \rightarrow 0$, $R_{\min} \rightarrow R_{\max}$).

$$\lim_{S \rightarrow 0} I = I_0 = \lim_{S \rightarrow 0} \frac{A(t)Y}{8\pi SD} \ln \frac{(D+S)}{(D-S)} = \frac{A(t)Y}{4\pi D^2}, \quad (11)$$

which is the correct result for radiation from a point source. A similar situation also arises for very long times (i.e., $S \gg D$, $R_{\min} \rightarrow R_{\max}$). The limit is:

$$\lim_{\frac{D}{S} \rightarrow 0} I = I_{\infty} = \lim_{\frac{D}{S} \rightarrow 0} \frac{A(t)Y}{8\pi SD} \ln \frac{(S+D)}{(S-D)} = \frac{A(t)Y}{4\pi S^2}, \quad (12)$$

which is the expected result for dose rate at the center of a spherical shell of activity $A(t)$ and radius S from a burst of yield Y .

The debris radiation relationship also exhibits a singularity when the shell crosses the asset. This singularity is not a numerical issue, but rather is caused by immersing the point detector in the radiating debris. For an actual asset, there is a finite size such that R_{\min} never goes to zero. This minimum radius can be considered to be the radius of the satellite. Simply adding the radius to the denominator is sufficient to suppress the singularity and will have no significant effect on the dose rate. The dose rate then becomes

$$I = \frac{A(t)Y}{8\pi SD} \ln \left(\frac{S+D}{|S-D|+r} \right),$$

$$I = \frac{A(t)Y}{8\pi SD} \ln \left(\frac{R_{\max}}{R_{\min}+r} \right). \quad (13)$$

This final result is the radiation environment caused by a single expanding shell for all values of time.

A dimensionless time variable may be introduced to parameterize the above relationships. The dimensionless time z is defined as

$$z = \frac{vt}{D} = \frac{S}{D}. \quad (14)$$

Substituting:

$$I = \frac{A(t)Y}{8\pi z D^2} \ln \left(\frac{1+z}{|z-1| + \frac{r}{D}} \right). \quad (15)$$

Combining the yield relationship for Equation (2) with the activity relation of Equation (1):

$$\frac{YA(t)}{R^2} = \frac{GF}{J(1+t)^{1.2}}. \quad (16)$$

The dose rate, I , can be rewritten as a function of prompt x-ray fluence rather than yield and distance to the burst, and t can be replaced by zD/v :

$$I = \frac{GF}{8\pi zJ \left(1 + z \frac{D}{v}\right)^{1.2}} \ln \left(\frac{1 + z}{|z - 1| + \frac{r}{D}} \right) \quad (17)$$

Now the dose rate is a function of the x-ray fluence, dimensionless time, and the characteristic time (D/v); it is also a very weak function of the distance to the burst and the satellite radius. For all practical purposes, r/D can be ignored or, at most, set equal to a constant. A reasonable value for r/D would be 10^{-5} corresponding to a 1-meter asset radius at a distance of 100 km. An order of magnitude change in r/D would typically change the dose by a factor of 2 for about 10 μ s, so selection of r/D is not critical, and for $|z - 1| \gg 10^{-5}$, r/D can be ignored.

A parametric plot of the background radiation is presented in Figure 2. The figure shows a family of curves for characteristic time (D/v) ranging from 0.01 to 100 s. The curves are normalized by dividing by the fluence, F , so that the units of the ordinate, MeV/(cal \cdot s) must be multiplied by the received fluence in cal/cm² to yield a debris dose rate in MeV/(cm² \cdot s).

An example application of this curve would be to determine the dose rate 3 s after a 1-MT burst occurring at a distance of 100 km with a debris velocity of 10^6 m/s. The resulting fluence is 0.64 cal/cm² (6.4×1000 kT/(100 km)²). The characteristic time is 0.1 s (100 km/ 10^6 m/s). The dimensionless time corresponding to 3 s is 30 (3 s/0.1 s). Reading the 0.10 s curve at $z = 30$, the dose rate is 8.5×10^7 MeV/s \cdot cal, which for 0.64 cal/cm² corresponds to 5.4×10^7 MeV/(cm² \cdot s). Specific plots can also be constructed by substituting the appropriate values into Equation (17).

4. MULTIBURST BACKGROUND ENVIRONMENT

The previous derivation describes the dose rate environment resulting from a single burst. When multiple bursts occur, the dose rate caused by the bursts will add. One way to estimate the dose rate from multiple bursts is to assume that a number of similar, regularly spaced bursts occur. This is only one of any number of burst scenarios. However, the result is useful since it provides a parametric solution to multiburst phenomena. By a number of similar bursts, it is implied that all bursts provide the same x-ray fluence and have the same characteristic time (distance from the asset). If m bursts occur during the characteristic time D/v , then the spacing in dimensionless time is $1/m$.

The background radiation level will vary with time as shells pass the asset, and the relative locations of shells change because a rapid change in dose rate occurs after shell passage. However, an average background dose rate can be determined. The multiburst environment can be envisioned as consisting of a number of equally spaced points, $1/m$ dimensionless time units apart, on the single burst background environment plot (Figure 2). Each of these points on the plot represents a source for the multiburst environment. As time passes, the points move right until at $1/m$ greater dimensionless time, the pattern repeats. Since all the equally spaced points exactly cover the curve every $1/m$ time period, the dose received per $1/m$ time during the engagement is the integral of the plot. So the dose rate is the integral multiplied by m , the dimensionless burst frequency. While this is an asymptotic dose rate, achieved exactly only for an infinite number of bursts,

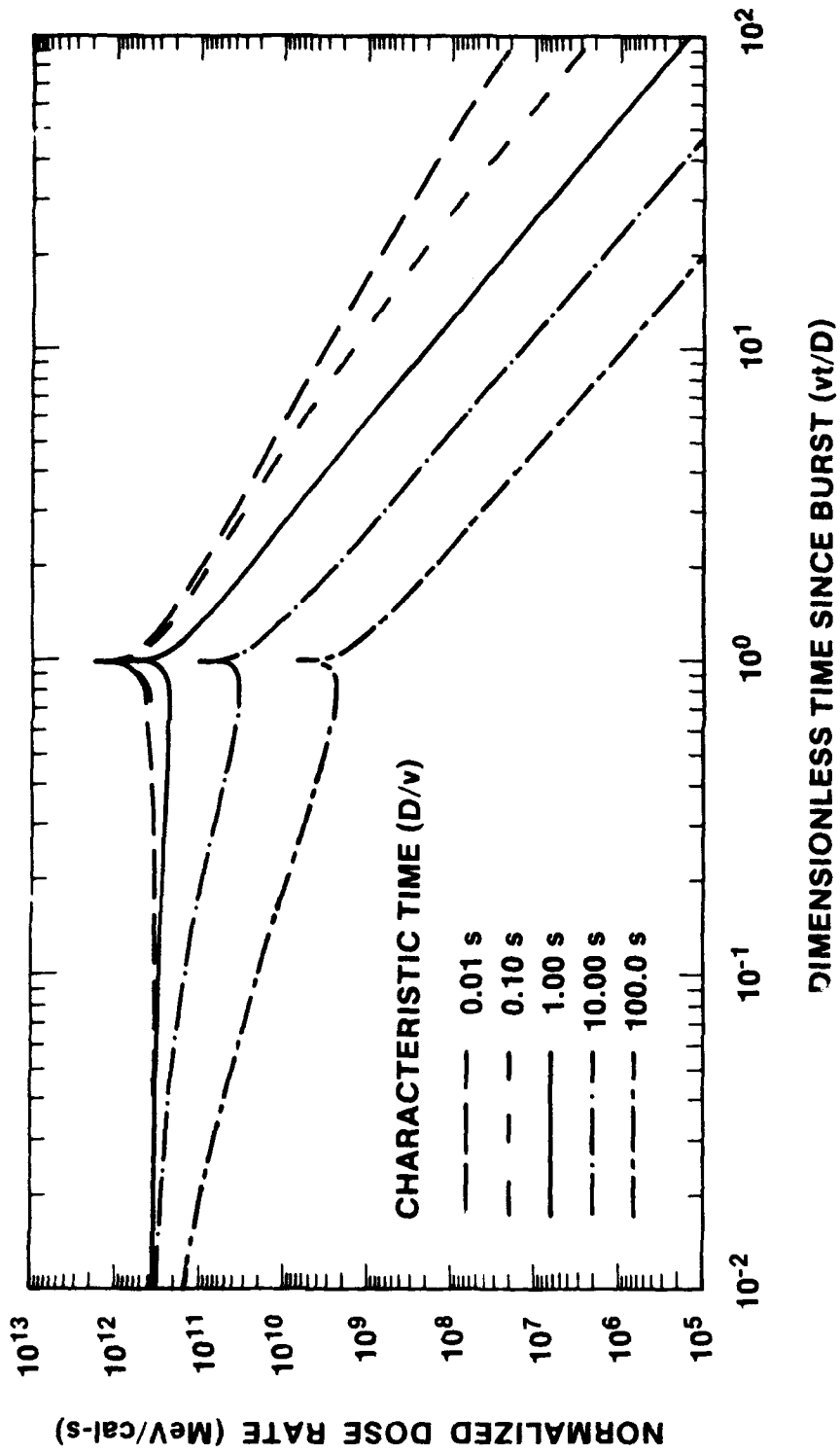


Figure 2. Single Burst Background Debris Environment

the rapid decrease in dose contribution for shells far from the assets allows this method to accurately estimate the dose rate for any multiburst scenario.

A relation for the normalized dose rate (i.e., not multiplied by m) is shown in Equation (18):

$$I = \int_0^{\infty} \frac{GF \ln\left(\frac{1+z}{|1-z| + r/D}\right)}{8\pi z J \left(1 + z \frac{D}{v}\right)^{1.2}} dz \quad (18)$$

Recalling that $z = vt/D$, the units of the integral can be converted to MeV/cal by multiplying by the characteristic time, D/v .

The results of the integration are presented in Figure 3. The units of the ordinate, MeV/cal, arise from the dose-rate contribution, $\text{MeV}/(\text{cm}^2 \cdot \text{s})$, that occurs from a flux in $\text{cal}/(\text{cm}^2 \cdot \text{s})$, which is periodically repeated. For long characteristic time, the dose per burst is higher. This is due to the fact that the majority of the dose occurs before the shell passes ($z < 1$), so long characteristic time provides extended periods of high dose rate. The values obtained can be multiplied by mv/D (the bursts per second) and the burst fluence in cal/cm^2 to determine the dose rate for a given threat environment.

The dose rate integral, Equation (18), left in dimensionless time, that is, not multiplied by D/v , results in units of $(\text{MeV} \cdot \text{characteristic time})/(\text{cal} \cdot \text{s} \cdot \text{burst})$ and can be multiplied by the bursts per characteristic time, m to determine the normalized dose rate. This plot is presented in Figure 4.

By using the previous example, a value of about 10^{12} $(\text{MeV} \cdot \text{characteristic time})/(\text{cal} \cdot \text{s} \cdot \text{burst})$ can be read from Figure 4 at characteristic time of 0.1 s. Choosing a burst rate of 1/s (0.1 per characteristic time), and $0.64 \text{ cal}/\text{cm}^2$ yields $6.4 \times 10^{10} \text{ MeV}/(\text{cm}^2 \cdot \text{s})$ as the continuous multiburst background dose rate. The plot in Figure 3 can also be used to determine the dose rate by reading $10^{11} \text{ MeV}/\text{cal}$ at a characteristic time of 0.1 s and multiplying by 1 burst/s and $0.64 \text{ cal}/\text{cm}^2$, yielding $6.4 \times 10^{10} \text{ MeV}/\text{cm}^2$.

5. PLATEOUT RADIATION ENVIRONMENT

Upon passing the space-based asset, weapon debris may plate out upon the surface of a satellite and cause a continuing source of radiation. Using the environment determined from the previous sections, the level of this plateout radiation may be estimated. A basic assumption for this determination is that the satellite gathers weapon debris from the portion of the passing shell that is equivalent to its projected area. The activity of the asset surface is increased by the activity of the passing shells, and the radiation source decays in intensity in the same manner as the shell from which it was deposited.

A detailed determination of the plateout radiation dose rate is dependent on asset geometry, requiring the deposition density in the projected area to be determined and the dose rate to be calculated to a specific point. For the purposes of determining an approximate dose rate, the asset will be assumed

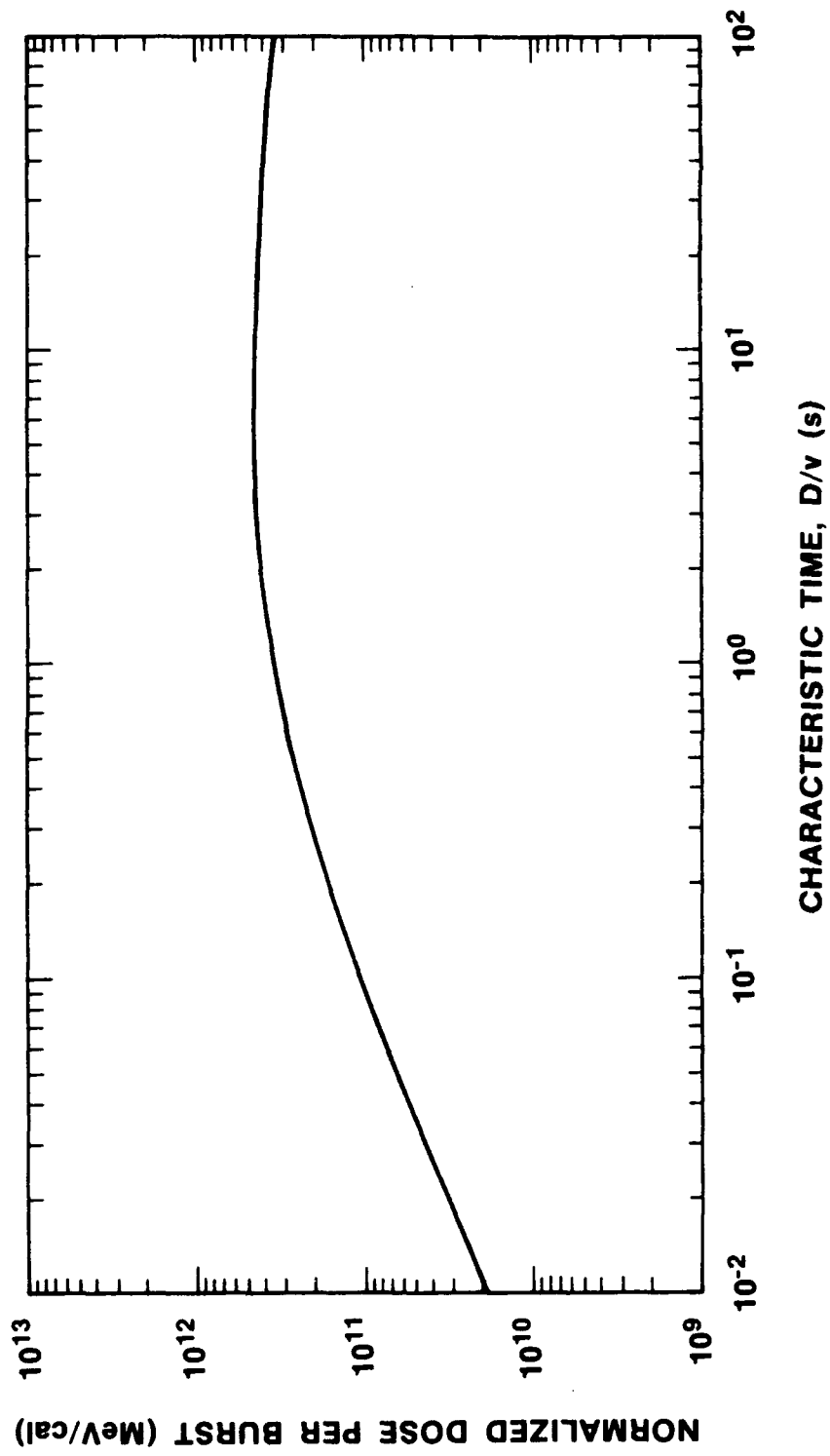


Figure 3. Multiburst Background Debris Environment

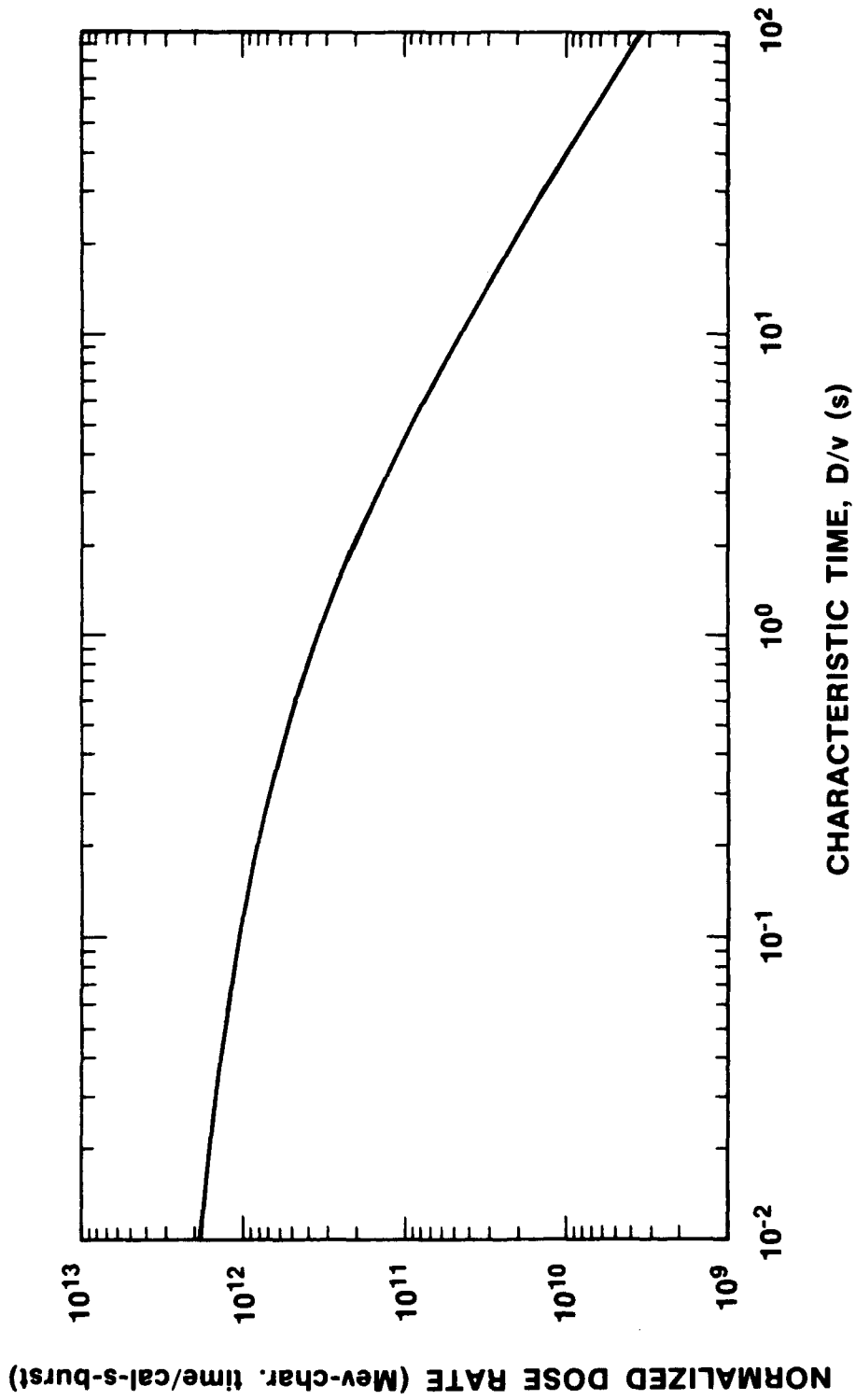


Figure 4. Parametric Multiburst Background Debris Environment

to be spherical in shape with a radius r , and the point of interest will be the center of the sphere. This will result in a dose rate that may well be slightly lower than that of an actual configuration but should not differ significantly in terms of the effect that the dose has on the assets. From before, the activity of the shell when it impacts the asset is

$$K(t) = \frac{A(t)Y}{4\pi S^2}, \quad (4)$$

$$YA(t) = \frac{GR^2F}{J(1+t)^{1.2}}. \quad (16)$$

This results in

$$K(t) = \frac{GF}{4\pi J(1+t)^{1.2}}. \quad (19)$$

Since this activity plates out on half of the spherical surface, the dose rate is

$$P = \int_0^{\pi/2} \frac{K(t)}{4\pi r^2} 2\pi r^2 \sin\theta d\theta = \frac{1}{2} K(t)$$

$$= \frac{GF}{8\pi J(1+t)^{1.2}}. \quad (20)$$

This is independent of the asset size.

This can be cast directly into dimensionless time, z , and characteristic time, D/v . Although this does not simplify the relationship, the result will be used later:

$$P = \frac{GF}{8\pi J \left(1 + z \frac{D}{v}\right)^{1.2}}. \quad (21)$$

Equation (20) is plotted in Figure 5. For comparison to the previous relationships using characteristic time, Equation (21) can also be used. The normalized dose rate in Figure 5 can be multiplied by the x-ray fluence in cal/cm^2 to yield the actual dose rate. Equation (20) must be used with some caution however, since the shell does not arrive until $t = D/v$; it should be rewritten as

$$P = \frac{GF u(t - D/v)}{8\pi J(1+t)^{1.2}}, \quad (22)$$

where $u(t)$ is the unit step function.

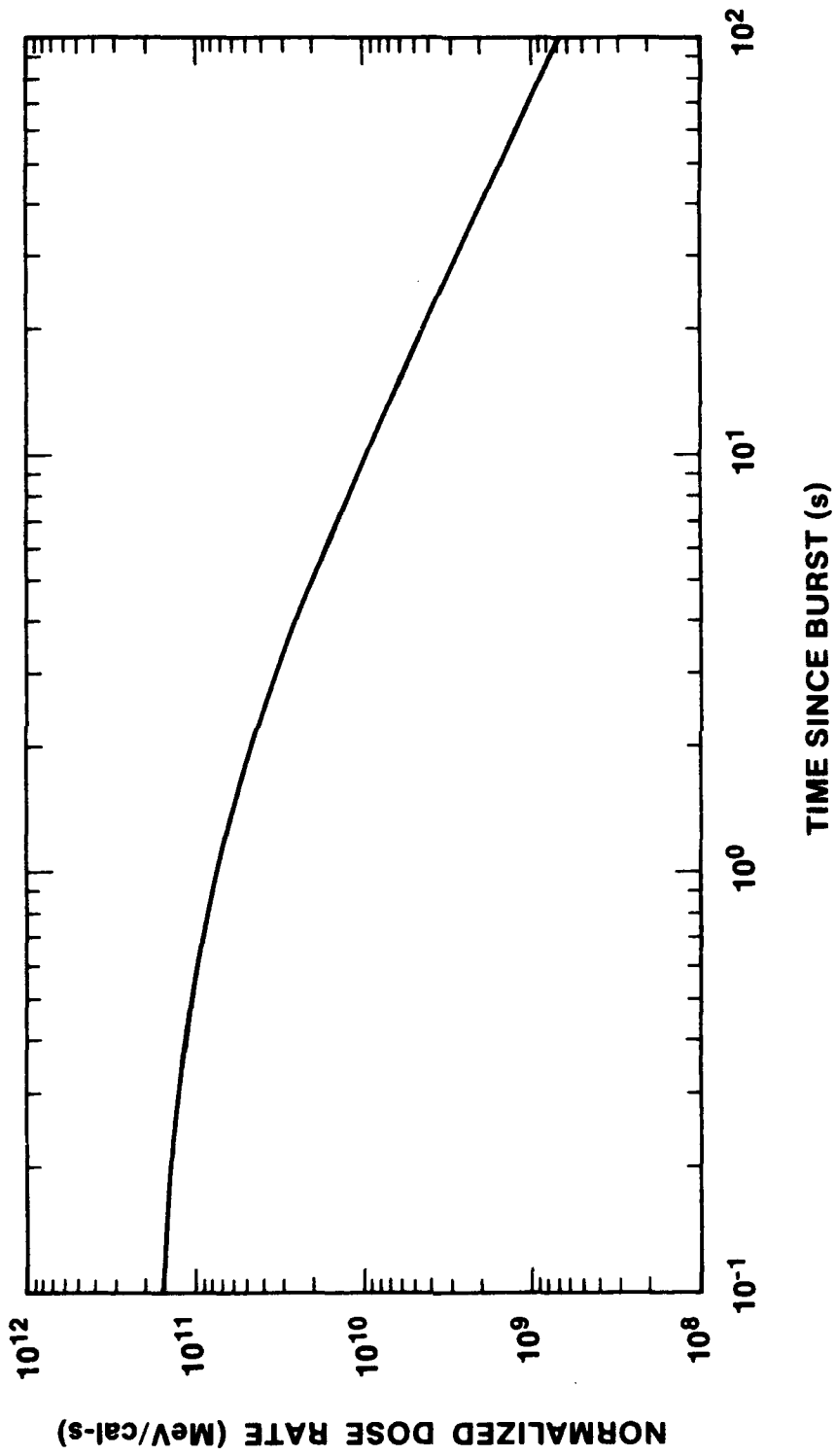


Figure 5. Single Burst Plateout Debris Environment

Equation (21) is shown in Figure 6 for a range of characteristic times. The minimum dimensionless time shown is 1 since the plateout always reaches the asset at $z = 1$.

Using the previous example, which resulted in 0.64 cal/cm^2 of fluence, the plateout from the burst at 3 s is $3.3 \times 10^{10} \text{ MeV/(s}\cdot\text{cal)}$. This can be read directly from Figure 5 or from Figure 6 after converting to dimensionless time of 30. Multiplying by the fluence results in $2.1 \times 10^{10} \text{ MeV/(cm}^2\cdot\text{s)}$.

6. MULTIBURST PLATEOUT ENVIRONMENT

As with the background radiation, the multiburst plateout scenario creates a more severe environment. The technique for summing the contributions of multiple debris deposition is similar to that described before. Again, the multiburst scenario consists of m bursts per characteristic time, D/v . The single burst plateout, P , is

$$P = \frac{GF}{8 \pi J \left(1 + \frac{D}{v} z\right)^{1.2}} \quad (23)$$

with $z = 1$ being the minimum time for the expression. As before, the multiburst environment can be determined by integrating the single burst expression and multiplying by the appropriate burst frequency. The integration must start at $z = 1$:

$$P = \int_1^{\infty} \frac{GF}{8 \pi J \left(1 + \frac{D}{v} z\right)^{1.2}} dz \quad (24)$$

$$= \frac{5vGF}{8 \pi DJ \left(1 + \frac{D}{v}\right)^{0.2}} \quad (25)$$

The resulting units are as before, $(\text{MeV}\cdot\text{characteristic time})/(\text{cal}\cdot\text{s}\cdot\text{burst})$. Equation 25 is plotted in Figure 7. Multiplying by the dimensionless burst rate, m , results in

$$P = \frac{5GFm}{D/v \ 8 \pi J \left(1 + \frac{D}{v}\right)^{0.2}} \quad (26)$$

The environment can also be converted to terms of MeV/cal by multiplying Equation (25) by the characteristic time. The resulting units are then MeV/cal and represent the gamma dose rate in $\text{MeV}/(\text{cm}^2\cdot\text{s})$ per x-ray dose rate in $\text{cal}/(\text{cm}^2\cdot\text{s})$. This result is shown in Figure 8.

The following example is presented to illustrate the use of Figures 7 and 8. Assume a multiburst scenario of a 1 MT burst each second at a range of 100 km [$0.64 \text{ cal}/(\text{cm}^2\cdot\text{s})$]. Further, use a characteristic time of 0.1 s ($v = 10^6 \text{ m/s}$). From Figure 7, the dose rate is $8.5 \times 10^{12} \text{ (MeV}\cdot\text{char. time/cal}\cdot\text{s}\cdot\text{burst)}$. The x-ray fluence is 0.64 cal/cm^2 occurring at a rate of 0.1

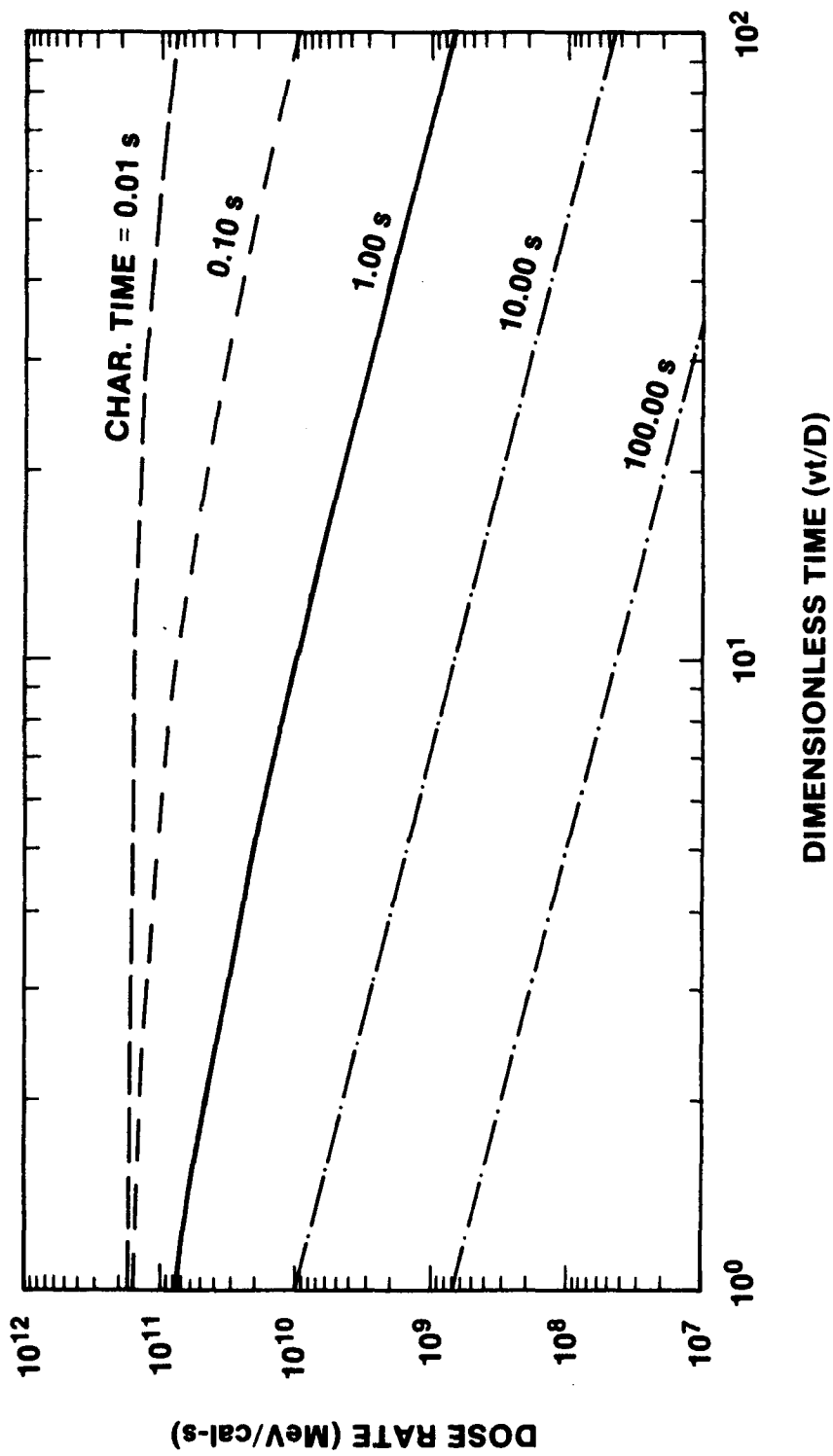


Figure 6. Parametric Single Burst Plateout Debris Environment

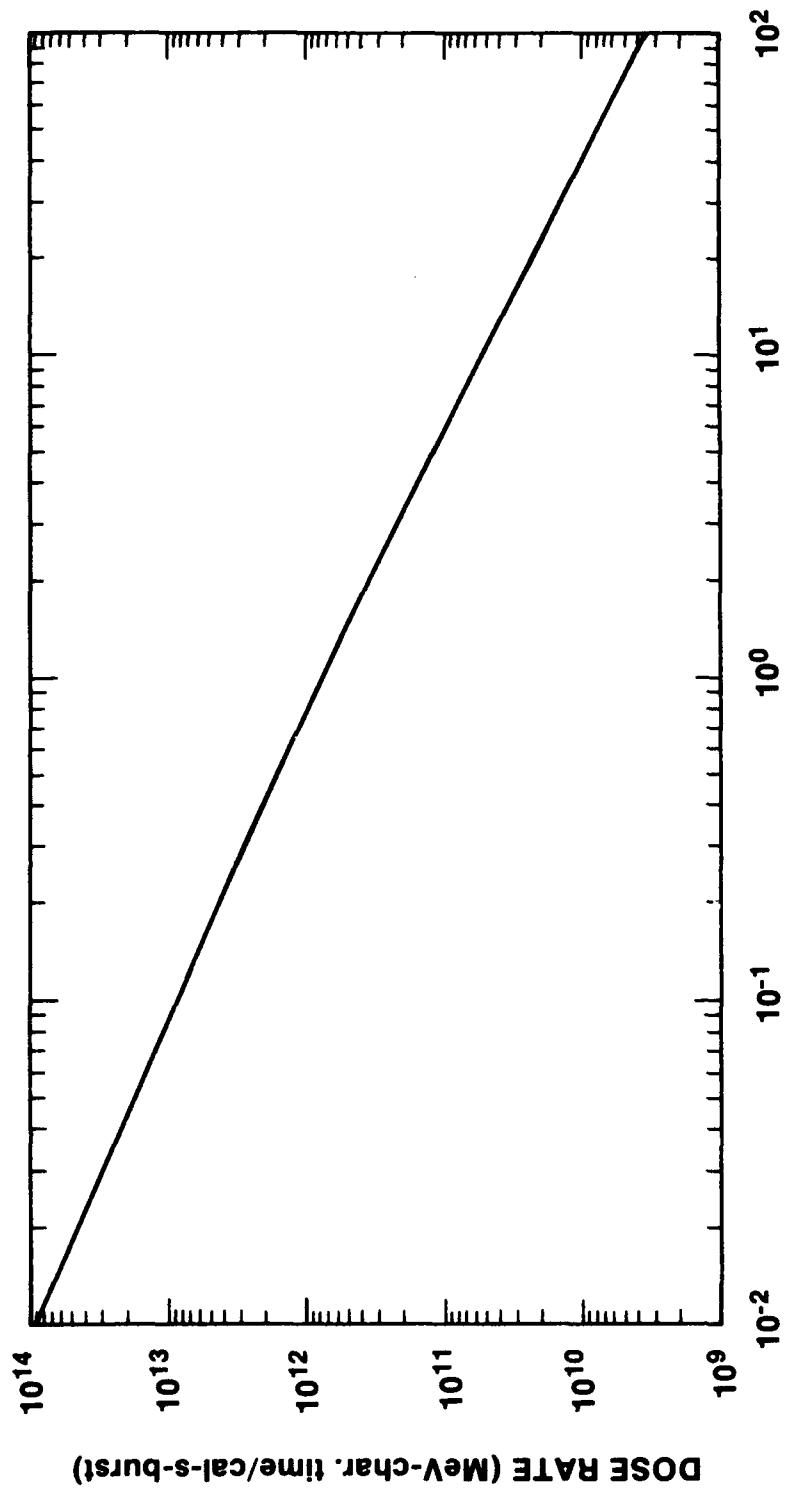


Figure 7. Parametric Multiburst Plateout Debris Environment

burst/char. time. This results in 5.4×10^{11} MeV/(cm²·s). Using Figure 8 for the same example, a dose per burst of 8.5×10^{11} MeV/cal can be read at the characteristic time of 0.1 s; multiplying this by 0.64 cal/(cm²·s) results in 5.4×10^{11} MeV/(cm²·s). Since Figure 8 exhibits only a weak dependence on characteristic time, a reasonable estimate of the multiburst plateau environment can be made as

$$P = 8.5 \times 10^{11} F n (\text{MeV}/\text{cm}^2 \cdot \text{s}) , \quad (27)$$

where F is the fluence in calories per cm² and n is the bursts per second.

Given the assumptions involved in satellite geometry, debris velocity, and debris activity, this single relationship is considered adequate for multiburst plateau environment determination.

The initial assumption for determination of the multiburst environment, both plateau and background, was that the bursts occurred at regular intervals, provided equal fluence, and had the same characteristic times. Both multiburst environments have been shown to be relatively insensitive to characteristic time and have been normalized to give the debris gamma dose rate as a function of the time-averaged prompt x-ray dose rate. Therefore, it is reasonable to assume that the relationships presented here are reasonably accurate for many general multiburst scenarios. As an upper bound, the general multiburst environment can be determined using the minimum expected time between bursts.

7. COMBINED DEBRIS RADIATION ENVIRONMENT

The previous derivations have resulted in the generation of plots representing the plateau and background debris radiation environment for both single burst and multiburst scenarios. The plots for the plateau and background radiation can be summed together to determine the total environment for both the single burst and multiburst scenarios. Figure 9 shows the result of this summing as a plot of the total debris radiation environment resulting from a single burst. The dose rate is again normalized to the x-ray fluence such that multiplying the value taken from the graph by the total x-ray fluence will yield the dose rate as a function of time in MeV/(cm²·s). By examining this plot and the two contributing plots that are added to form this one, it can be seen that the dominant source of radiation changes in the region of dimensionless time are equal to 1 or 2, after the expanding debris shell passes the space-based asset. Specifically, before the debris shell reaches the asset, the radiation environment consists solely of the background radiation because no plateau is yet available. When the plateau is on the surface of the satellite, the radiation fluence begins to be dominated by the plateau debris as the expanding shell moves away from the asset. For values of z away from the region of $1 < z < 2$, a very good approximation for the dose rate may be determined. Specifically, for values of z substantially less than 1, the dose rate from the expanding shell presented in Equation (17) becomes

$$I = \frac{GF}{4\pi J(1 + \tau)^{1.2}} \quad (28)$$

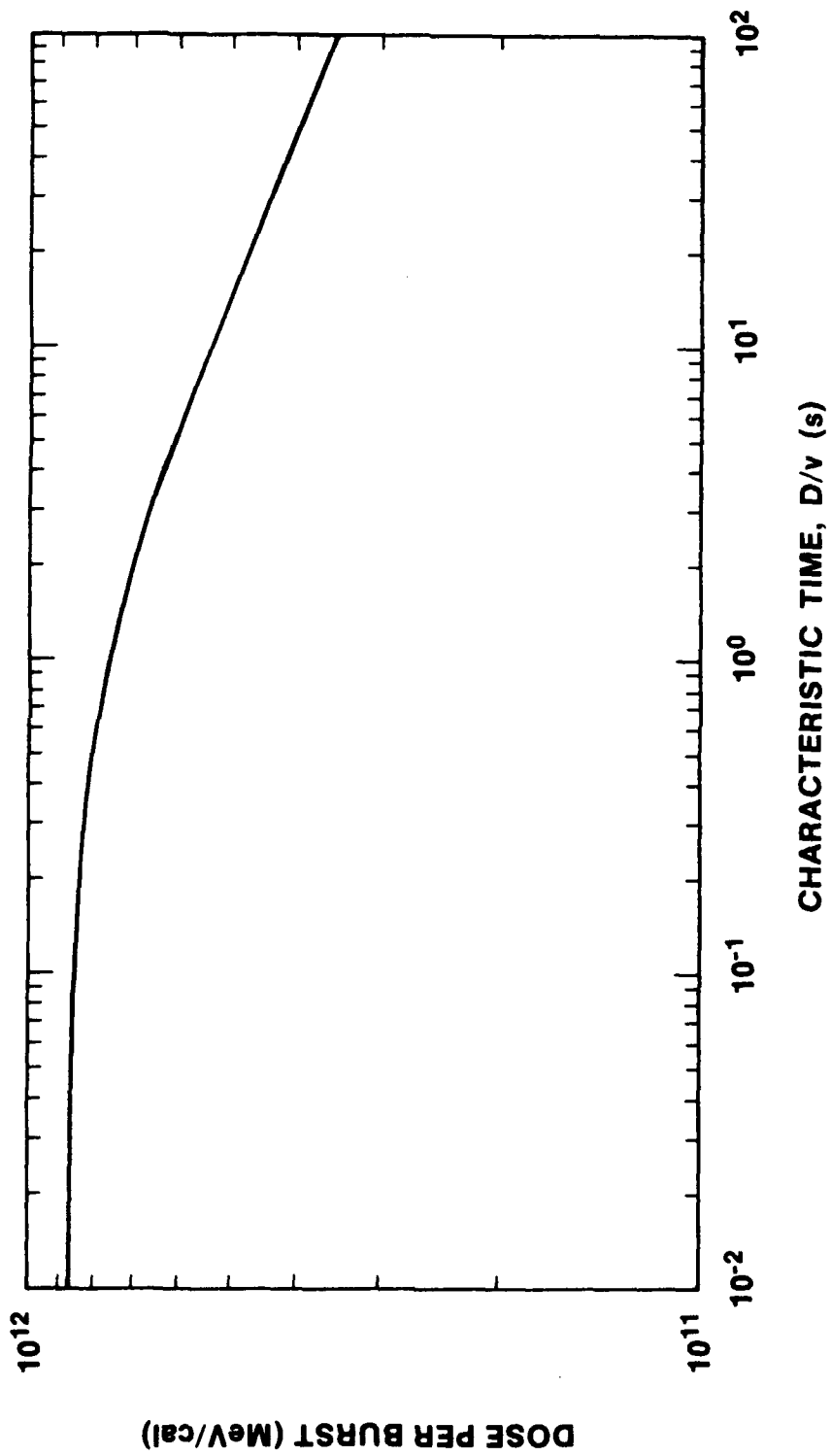


Figure 8. Multiburst Plateout Debris Environment

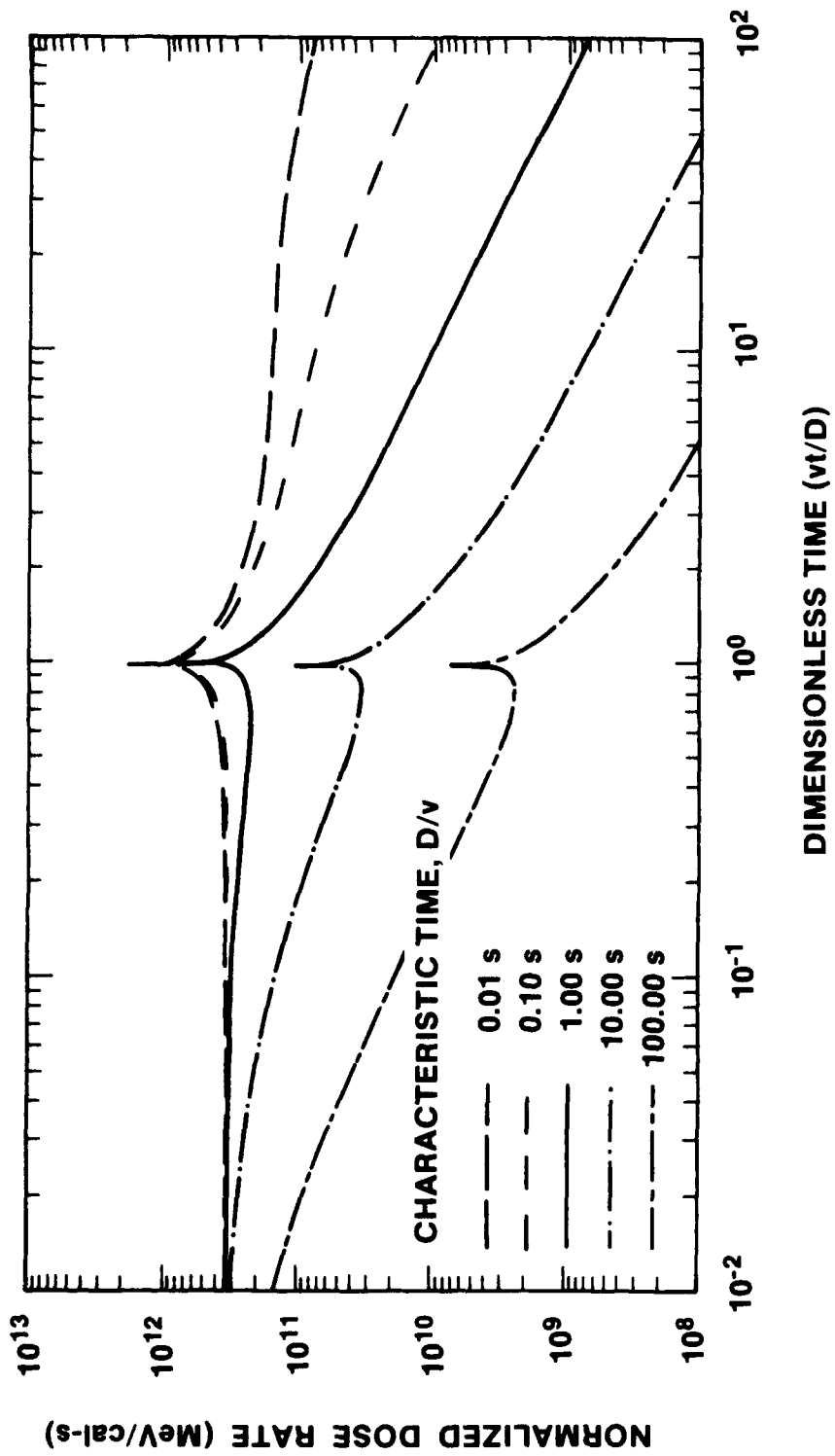


Figure 9. Single Burst Total Debris Environment

And for large values of z , the equation previously derived for the plateau debris radiation, Equation (20), is appropriate, and is repeated here:

$$P = \frac{GF}{8\pi J(1 + t)^{1.2}} \quad (20)$$

These two equations differ from each other by a constant value of 2, and by examining the original equations cast in terms of dimensionless time z , it can be shown that the contributions of the two separate equations are the same at $z = 2$. Therefore, the two can be combined using a unit step function giving a single relationship for the dose rate at all times. The relation is as follows:

$$R = \frac{GF(u(2 - z) + 1)}{8\pi J(1 + t)^{1.2}} \quad (29)$$

For a specific characteristic time of 1 s, the calculated dose rate, as well as the approximation shown in Equation (29), is plotted and shown in Figure 10. Notice that with the exception of a time when the debris wave passes the spacecraft, this approximation provides very good correlation with the calculated dose rate. One final issue, with regard to the single burst dose rate, is determining the upper bound of the dose rate at the time $z = 1$. This relationship comes directly from substituting $z = 1$ into the expression for the background debris dose resulting in

$$I_{\max} = \frac{GF}{8\pi J \left(1 + \frac{D}{v}\right)^{1.2}} \ln(2D/r) \quad (30)$$

This can be seen to have a considerable dependence on the satellite radius, but for typical values of burst distance and satellite radius, the logarithm in the previous equation will have an approximate range of from 6 to 16 resulting in a peak dose that is three to eight times higher than the dose predicted by the approximated dose rate equation. This dose, however, does not last for more than approximately 0.1 characteristic times, on either side of $z = 1$.

A combined plot for the multiburst environment can also be constructed where the contributions caused by the multiburst plateau environment (Figure 8) and the multiburst background environment (Figure 3) are summed to produce a single total environment plot. This plot is shown in Figure 11. Since the calculated environment varies by less than a factor of 2 over a 4-order of magnitude variation in the characteristic time, a constant value for the dose rate of 10^{12} MeV/cal is appropriate. Multiplication of the value from the graph by the cal/cm² of x-ray fluence, F , and by the number of bursts per second, n , directly yields the dose rate in MeV/(cm²·s) that will occur in a steady-state multiburst scenario. The total multiburst relation is

$$I = 1.0 \times 10^{12} F n \quad [\text{MeV}/(\text{cm}^2 \cdot \text{s})] \quad (31)$$

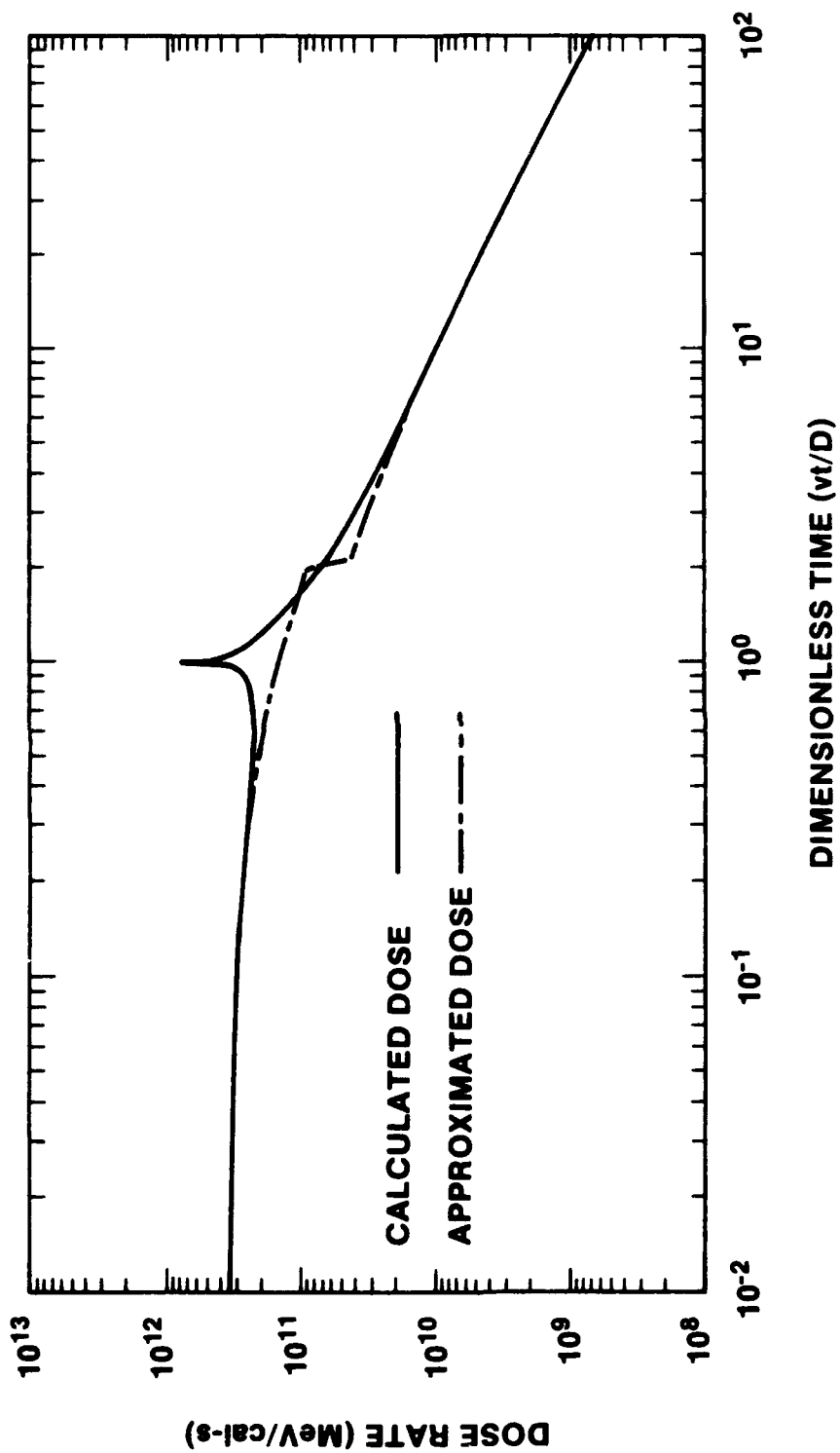


Figure 10. Comparison of Calculated and Approximated Dose Rates for a Single Burst With $Z = 1$ s

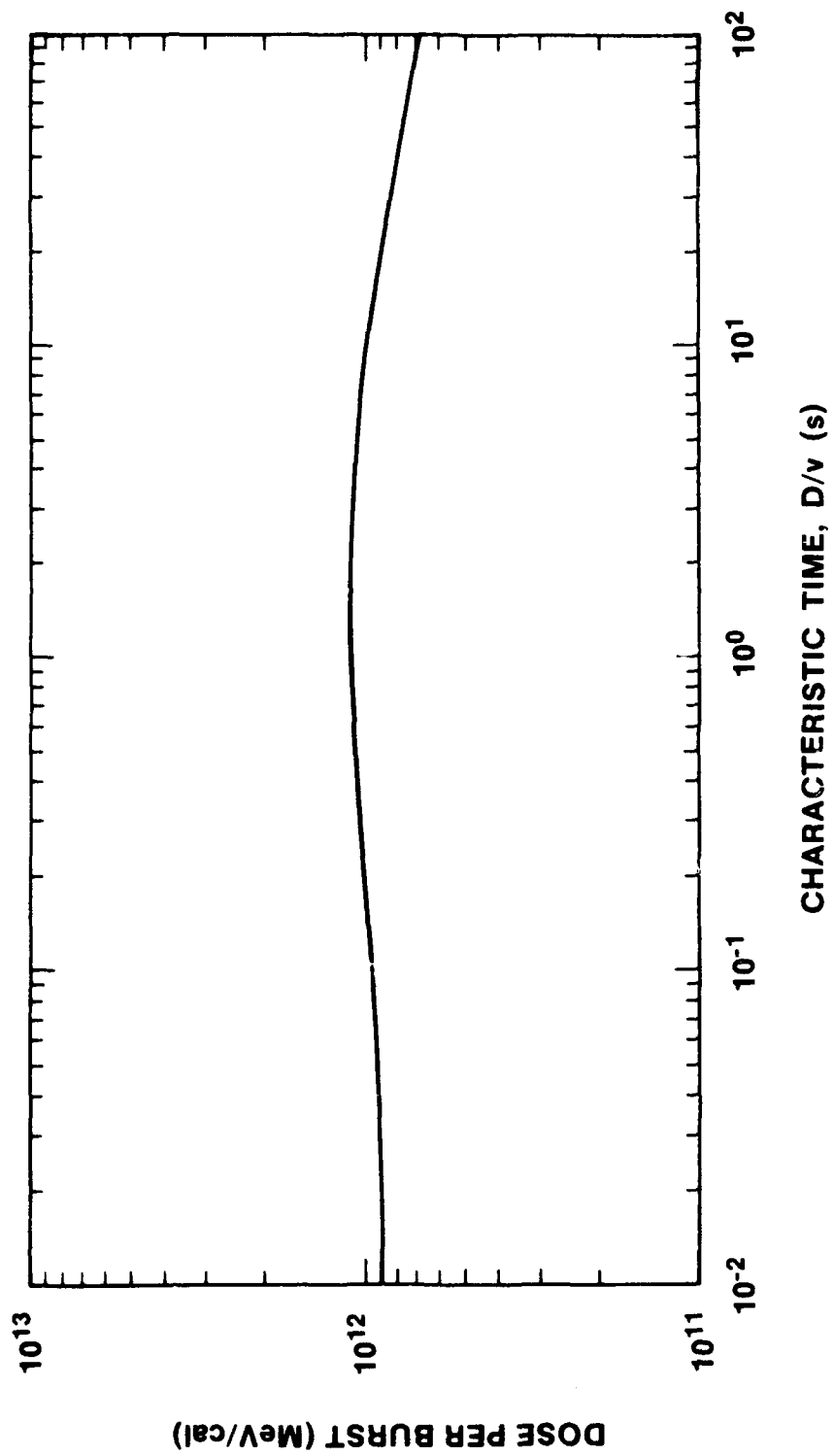


Figure 11. Multiburst Total Debris Environment

8. DEBRIS ENVIRONMENT APPLICATION

The previous plots give sufficient information to determine the debris dose received by a satellite in both background and plateout conditions for single and multiburst environments. All doses have been discussed in terms of $\text{MeV}/(\text{cm}^2 \cdot \text{s})$. This is the external free-field environment that would be seen in the region of the satellite. This can be converted directly to rads by using a typical cross section of approximately $0.03 \text{ cm}^2/\text{g}$ for silicon and by using the fact that a typical energy of the debris gamma is approximately 0.7 MeV. This cross section is valid from 200 keV to 1 MeV. The following sections discuss the implications of the debris radiation environment and consider the problems of shielding sensitive areas, such as the electronics, and operating during this environment.

9. MITIGATION OF DEBRIS RADIATION ENVIRONMENT

Using the previous derivations, the debris radiation environment is on the order of $3 \times 10^{11} \text{ MeV}/(\text{cm}^2 \cdot \text{s})$, for example, for a $1\text{-cal}/\text{cm}^2$ fluence or a multiburst scenario with one burst per 3 s [Equation (31)]. This number corresponds to approximately 150 rads/s for silicon in a free-field environment. Since these environments only last for a few minutes to hours at most, the total dose accumulated is of no concern with regard to most hardened electronics. Further, the dose rate is many orders of magnitude lower than that which could be considered damaging to electronic parts. However, the debris radiation environment is of primary concern with regard to sensor detectors. It is particularly true of optical detectors such as focal plane arrays. The debris radiation on these detectors causes significant noise in the signal that must be considered.

It is essential that some action be taken to mitigate the debris radiation. Two general techniques are recognized for designing against radiation. The first is direct shielding where a relatively massive shield is required to attenuate the radiation such that the level transmitted is within the threshold of the sensors. The second method is to remove the radiation from the surface of the space based asset. This only removes the plateout radiation source and has no effect on the background radiation levels. However, for a relatively long time after bursts, the plateout radiation tends to dominate the debris radiation environment such that there are periods of time when removal of the plateout radiation could be very useful. These two methods of debris radiation mitigation are discussed below.

Using shielding to attenuate debris radiation tends to require relatively large quantities of shield mass. A shield mass required to provide a specific attenuation is, of course, dependent on the energy absorption cross section of the material chosen for a shield. Glasstone¹ gives an approximate average energy for debris radiation of about 700 keV. However, the energy from a given threat must be specifically determined, since the average energy can range from approximately 500 to 1000 keV.

To shield against this background radiation, a small spherical shield can be envisioned that encompasses the focal plane array and leaves open only the acceptance angle of the array. An active shield that closes during periods of susceptibility could also be envisioned, although its cost would be substantially higher. This open acceptance angle does allow for some direct

radiation to the array and therefore limits the effectiveness of the shield applied to the rest of the area. However, for relatively narrow field-of-view sensors, this may be acceptable. For example, for a five-degree field-of-view sensor, the area open is approximately 0.1% of the total area to be shielded allowing shield effectiveness of up to 3 orders of magnitude. Likewise, for a 15-degree angle of view, shielding of up to 2 orders of magnitude can be accomplished.

To accomplish this shielding with minimum weight, uranium is the most effective material. This is due to the relatively high density and high cross section of uranium. Uranium has about a 50% greater cross section than lead. However, it does provide a background radiation consisting primarily of 47-keV photons with an intensity of approximately 1000 photons per cm^2/s . If a continuous background level of this magnitude is a problem, a $1\text{-g}/\text{cm}^2$ lead shield can be applied inside the uranium shield to give a 3 order of magnitude attenuation for this radiation.

The amount of uranium necessary to shield a 1-cm-diameter sphere (the size of a small focal plane array) and provide 1 order of magnitude attenuation against 700-keV photons is 680 g. Likewise, for a 2 or 3 order of magnitude attenuation, the required mass is 3.8 and 11.0 kg. The various shield weights needed for a uranium shield around the 1-cm sensor with varying photon energies of 500 to 1000 keV are shown in Figure 12. While these weights are not insignificant, they may be considered feasible with regard to protection of small focal plane arrays on sensor platforms.

There are three general areas where the use of heavy attenuation shielding is not considered feasible: (1) the space-based interceptor, in which mass is at an extreme premium; (2) wide angle field-of-view sensors, in which shielding the bulk of the surface with a thick attenuation shield is not practical; and (3) large focal plane arrays for which the shielding weight becomes exorbitant. In such areas, the combination of hardened sensor arrays with less massive shielding may be the only acceptable alternative.

The second method for mitigating the debris radiation environment involves removal of the plateout debris from the surface of the space-based asset. Since this removal is much more complex than simple attenuation shielding, and, further, is not capable of handling the background radiation environment, plateout debris removal should be considered only when absolutely necessary. Figure 5 shows that the single burst plateout environment is limited to about 10^{11} $\text{MeV}/(\text{cal}\cdot\text{s})$ and drops to 10^{10} $\text{MeV}/(\text{cal}\cdot\text{s})$ at 10 s after a burst. Since the decay of plateout debris continues at a logarithmic rate, a reduction in the debris amount by a factor of 10 will be needed to have any significant impact in the environment. In terms of removal of plateout debris from the surface of a space-based asset, this means that 90% of the debris must be removed. Based on the previous derivations of the plateout debris environment, the 90% removal refers to 90% of the solid angle viewed by the focal plane array, so it may be adequate to remove the plateout from a significantly smaller fraction spacecraft as long as the solid angle from the array meets the 90% criterion. As was mentioned

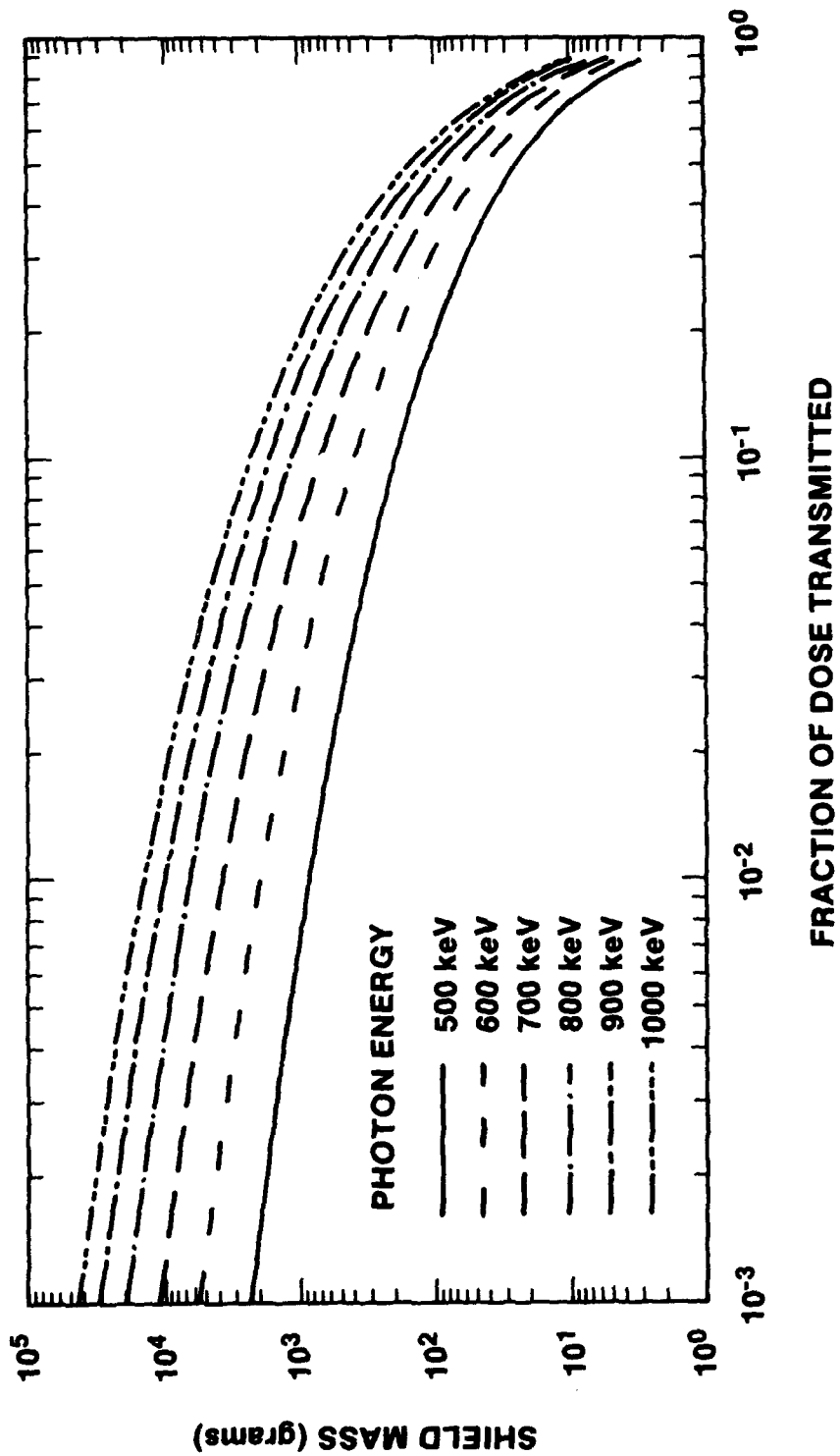


Figure 12. Required Uranium Shielding for a 1-cm Sensor

before, the debris radiation environment is dominated by the background environment up to characteristic time $z = 2$, the time when the debris shell has passed the spacecraft and is the same distance from the spacecraft as the initial burst. After this time, the dose received from the debris plateout quickly begins to dominate the debris dose environment.

A method of removing the plateout from the spacecraft would be employing shedable skins. These skins would consist of a thin outer layer, which is ejected from the spacecraft after the plateout debris arrives. This ejection can be accomplished any time between a dimensionless time of one when the debris has arrived and a dimensionless time of approximately 2 when the plateout debris begins to become the dominant radiation factor in the debris dose. On a generally cylindrical body, such as the space-based interceptor, this ejected skin would have the form of a sleeve covering the sides, but not the ends of the interceptor. This sleeve must be ejected at a velocity such that it moves away from the spacecraft to quickly reduce the dose caused by the plateout radiation. A membrane sleeve could be envisioned that is ejected by means of compressed gas used to inflate, burst, and accelerate the sleeve away from the spacecraft. Methods of releasing the shield from its attachment, if such attachments exist, would also need to be considered.

Assuming that such shedable skins can be developed, the focal plane array must still deal with the background environment. The worst case for the background environment involves short characteristic times on the order of 1 s or less. Such characteristic times are considered credible, since a 1-s characteristic time corresponds to a 0.6-cal/cm² fluence from a 1-megaton burst assuming a debris velocity of 10⁵ m/s. For higher debris velocities, larger fluences, or smaller yield weapons the characteristic time becomes less. For this characteristic time, the background debris radiation drops to the value of 10¹⁰ MeV/(cal·s) at dimensionless times of about seven. However, the longer the characteristic time, the more rapidly the environment, in terms of dimensionless time, decays to the 10¹⁰ level.

To examine the issue of the amount of time off-line for a detector following a burst, it may be useful to consider the effects of a specific yield threat. Consider, for example, a 1-megaton burst occurring at any of several distances from the asset. The dose-time plot can be determined directly from the previously derived equations. Since the burst yield is constant and various distances to the asset are being considered, the equations should be rewritten in terms of actual time rather than dimensionless time. This allows the dose-time plots for several different bursts to be compared. Rearrangement of the parametric equations for the background dose rate results in the following:

$$I = \frac{GY}{8\pi Dvt(1 + t)^{1.2}} \ln \left(\frac{vt + D}{|vt - D| + r} \right), \quad (32)$$

where the yield in kilotons, Y, has been reintroduced and the debris velocity v and a distance to the burst D have been included. For an assumed burst yield of 1 megaton and a velocity of the debris of 10^5 m/s, the plot presented in Figure 13 results. This plot shows an asymptotic behavior for all burst distances at characteristic times greater than 1 (to the right of the dose-rate peak caused by the passage of the debris front). The equation for the asymptote may be determined by allowing vt to become large in the previous equation. The result is

$$I_{LIM} = \frac{GY}{4\pi(vt)^2(1+t)^{1.2}}, \quad (33)$$

which may be used to determine the time at which the background dose rate falls below a certain predetermined level for any given yield and assumed debris velocity. Note here that the relationship is quite sensitive to debris velocity assumptions. In the previous plot, the assumed debris velocity of 10^5 m/s represents what has been previously determined to be a likely lower limit to debris velocity. As the velocity is allowed to increase to its upper limit of 10^6 m/s, the debris limit will decrease by 2 orders of magnitude. For any assumed threat yield and debris velocity, the time that a given sensor will be inoperable can be determined directly from Equation (33) or from Figure 13. If a single order of magnitude shield is provided, the off-line time is reduced by a factor of about 2.4 based on the time exponents of Equation (33). Further, for distant bursts there may be no off-line time caused by background debris radiation. In general, the distance at which a burst may occur and not cause an off-line period for a sensor can be determined by evaluating the background parametric dose rate equations for the condition $z = 0$. The result of this evaluation is

$$D = \sqrt{\frac{4\pi I_D}{GY}}, \quad (34)$$

such that for a given radiation tolerance of a sensor (I_D) and a yield of a burst (Y), the maximum distance of the burst of concern (D) can be determined.

10. SUMMARY AND CONCLUSIONS

Both the background and plateout debris gamma environments realizable from nuclear detonation can be of concern to sensitive electronics in space-based assets. Dose rates of 10^{11} MeV/($\text{cm}^2 \cdot \text{s}$) per cal/ cm^2 are obtained in multiburst engagements with 1 burst every 10 seconds. Single bursts can also provide debris dose rates of 10^{11} MeV/($\text{cm}^2 \cdot \text{s}$) per cal/ cm^2 for several seconds.

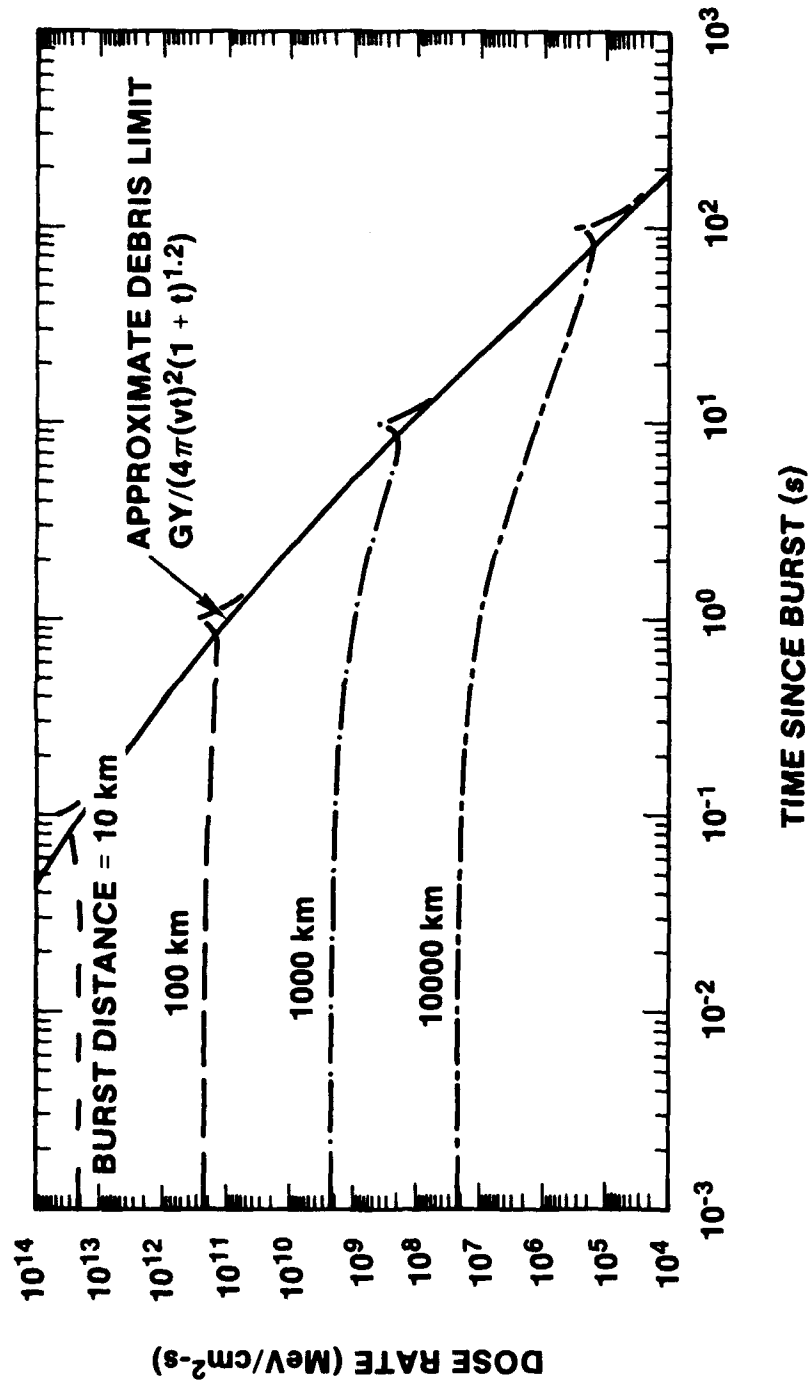


Figure 13. Background Debris Dose for a 1-MT Burst

The debris environment as derived and presented here shows that for focal plane arrays, the shielding of small detectors with limited fields of view is achievable by using attenuation shielding for sensor platforms. However, for the case of very large sensors, wide fields of view, or for sensors on interceptor vehicles, high hardness sensors and shielding will be necessary. In addition, a technique for the removal of plateout debris from the surface of the spacecraft may be required. While the requirement for shielding on interceptor vehicles and the development of shedable skins from the vehicle incur some mass penalty and additional complexity of the vehicle, it is considered feasible, and the weight penalties are generally not extreme.

11. REFERENCE

1. Samuel Glasstone and Philip V. Dolan, The Effects of Nuclear Weapons, 3rd Edition, U.S. Department of Defense and The Energy Research and Development Administration, Washington, D.C., 1977.

DISTRIBUTION LIST

Phillips Laboratory (12)

Attn: IMA for
NTC/Dr. C. Aeby
NTC/John Mullis
Lt. Mike Black
NTC/Lt. Col. Schneider
NTCA/ Mr. Dale Hilland
NTCA/Capt. J. Gray
NTCA/Dr. M. Harrison
NTCA/Dr. B. K. Singaraju
SW/Lt. Col. A. Alexander
SLW/Lt. Col. H. Pugh
SWW/Capt. J. Moody

Kirtland AFB, NM 87117-6008

SDIO (2)

The Pentagon, RM 1E178
Attn: Lt. Col. C. Hill/INK
Maj. Tom McDowell/INK
Washington, DC 20301-7100

Space System Division (4)

Attn: CNZ/Lt. Col. J. Ledbetter
CNBSS/Maj. L. Rensing
CNIWT/Capt. Simpson
CNSE/Capt. Howard

P.O. Box 92960
Los Angeles AF Station
Los Angeles, CA 90009-2960

USA Strategic Defense Command (3)

Attn: CSSD-H-MPM
For: CSSD-H-SAV/Dick Bradshaw
CSSD-H-LS/Ira Merritt

106 Wynn Drive
P.O. Box 1500
Huntsville, AL 35807-3801

Bettis Atomic Power Laboratory

Attn: Document Custodian
P.O. Box 79
West Mifflin, PA 15122-0079

U.S. Department of Energy
Albuquerque Operations Office

Attn: Library
P.O. Box 5400
Albuquerque, NM 87115

U.S. Department of Energy

Energy Library MA23221
Attn: T & A Station
P.O. Box A
Germantown, MD 20874

Los Alamos National Laboratory

Attn: Report Librarian
P.O. Box 1663
Los Alamos, NM 87545

JAYCOR

Attn: Dr. Burr Passenheim
For: Mr. Eric Wennas
P.O. Box 85154
San Diego, CA 92138-9259

Kaman Sciences Corp.

Attn: T. S. Pendergrass
P.O. Box 2486
Huntsville, AL 35804-2486

Mission Research Corporation

Attn: Toni Hensley
For: Mr. Bob Gardner
1720 Randolph Road SE
Albuquerque, NM 87106-4245

Science Applications Int'l Corp.

Attn: Donna Ovellette
2109 Air Park Road SE
Albuquerque, NM 87106

Science Applications Int'l Corp.

Attn: George Lockett
For: Mr. Bill Chadsey
P.O. Box 9870
McLean, VA 22102

S-Cubed, Division of Maxwell Labs

Attn: Document Control
For: John Uecke
P.O. Box 1620
La Jolla, CA 92038-1620

Booz-Allen and Hamilton Inc.

Attn: Mike Saunders
4330 East-West Highway
Bethesda, MD 20814

Grumman Aerospace Corporation
Attn: Marshall Jew (MS: A02-105)
CDC (Ms: A04-35)
Bethpage, NY 11714

Lockheed Missiles and Space Co.
Inc.
Attn: Document Control for Bldg.
593 (Jerry Jagers)
P.O. Box 3504
Sunnyvale, CA 94088

Martin Marietta Space Systems
Attn: Document Control for
Ron Boatwright MS-L-8030
P.O. Box 179
Denver, CO 80201

Administrator
Defense Technical Information
Center
ATTN: DTIC/FDAC
Bldg. 5
Cameron Station
Alexandria, Virginia 22304-6145

TRW, Inc.
Attn: Paul Chivington
Suite 200
2340 Alamo SE
Albuquerque, NM 87106

Defense Nuclear Agency (3)
Attn: SSAB
For: RAEE/Robert C. Webb
RAEE/Dr. Gracie E. Davis
6801 Telegraph Road
Alexandria, VA 23310-3398

Naval Research Laboratory
Attn: Code 4611/Ed Peterson
Washington, DC 20375-5000

The Aerospace Corporation (4)
Attn: Darlene S. Reams
For: MS M5-614/Cecil Crews
MS M7-597/P. Mahadevan
MS M2-241/Robert Cooper
MS M7-633/Dr. James Gee
P.O. Box 92957
Los Angeles, CA 90009-2957

U.S. Department of Energy
Office of Scientific & Technical
Information
P.O. Box 62
Oak Ridge, TN 37831

Computer Sciences Corporation
Attn: Library
2100 Air Park Rd. SE
Albuquerque, NM 87106

EOS Technologies Inc.
Attn: Dr. D. Payton
200 Lomas NW, Suite 1121
Albuquerque, NM 87102

University of California
Lawrence Livermore National
Laboratory
Attn: Technical Information Dept.
P.O. Box 808
Livermore, CA 94550

Martin Marietta Energy Systems
ORGDP Records Department
P.O. Box P
Oak Ridge, TN 37831

NASA Langley Research Center
Attn: Technical Library Branch
Mail Stop 185B
Hampton, VA 23665-5225

1541 R. J. Lawrence
5000 R. L. Hagenruber
6400 N. R. Ortiz
6501 J. V. Walker
6473 J. H. Lee, Jr.
6474 R. E. Pepping
6474 D. K. Monroe
6473 B. L. Spletzer (5)
6623 W. T. Wheelis
7141 S. A. Landenberger
(5 copies)
7151 G. C. Claycomb (3)
7613-2 Document Processing (8)
for DOE/OSTI
8523-2 Central Technical Files
9352 G. J. Scrivner